Journal of Hydrology 577 (2019) 123923

Contents lists available at ScienceDirect

Journal of Hydrology

journal homepage: www.elsevier.com/locate/jhydrol

Research papers

The utility of near-surface water vapor deuterium excess as an indicator of atmospheric moisture source

Zhongwang Wei[a,b,*], Xuhui Lee[a,c]

[a] School of Forestry and Environmental Studies, Yale University, New Haven, CT, USA
[b] River and Environmental Engineering Laboratory, Department of Civil Engineering, University of Tokyo, Tokyo, Japan
[c] Yale-NUIST Center on Atmospheric Environment, Nanjing University of Information Science & Technology, Nanjing, Jiangsu, China

ARTICLE INFO

This manuscript was handled by Marco Borga, Editor-in-Chief, with the assistance of Huade Guan, Associate Editor

Keywords:
Deuterium excess
Moisture source
Back trajectory
Kinetic fractionation

ABSTRACT

This study explores the utility of observations of deuterium excess (dx) of water vapor for attribution of vapor to remote source regions and local influences. A Lagrangian back trajectory model was combined with various parameterizations of the dx of ocean evaporation and land evapotranspiration to simulate daily vapor dx at a continental site, a marine site and a coastal site. The model reproduced reasonably well the observed variabilities in the vapor dx at the coastal and the marine site when water vapor at these sites were primarily influenced by large-scale advection from ocean sources. The simple parameterization relating dx of the ocean evaporation to relative humidity is a robust representation of the ocean isotopic evaporation. On the other hand, the model did poorly for the continental site and during the land evapotranspiration dominated months at the coastal and the marine site, confirming the published findings that the water vapor dx near the Earth's surface can be significantly altered by land evapotranspiration and therefore is not a conserved tracer of humidity from the marine moisture source region. Several parameterizations for the dx of land evapotranspiration suggested by previous studies were tested with the trajectory model, but none brought improvement to the simulation of the dx at the continental site. Our study emphasizes that a fundamental challenge in isotopy hydrology is the lack of understanding of the different fractionation processes of ^{18}O and D associated with land evapotranspiration.

1. Introduction

Water vapor isotopes (HDD and $H_2{}^{18}O$) in the atmospheric boundary layer have been widely used in tracing physical processes in hydrological and climatic studies (Aemisegger and Sjolte, 2018; Galewsky et al., 2016; Gat, 1996; Good et al., 2015; Jasechko et al., 2013; Wright et al., 2017). Variations in the abundance of these isotopes, expressed in delta-notation as δD or $\delta^{18}O$, result from equilibrium and kinetic fractionation associated with phase changes of water during land surface evapotranspiration, sub-cloud raindrop evaporation and in-cloud condensation and from mixing during atmospheric convection, boundary layer entrainment, and airmass advection. In these processes, the vapor δD or $\delta^{18}O$ is not conserved. For example, in the process of large-scale airmass advection, as the air mass dries out due to precipitation, the remaining vapor becomes progressively depleted in D and ^{18}O. The Rayleigh distillation model (Gat, 2000) predicts a reduction of 100 ‰ for δD at a dryout ratio of 0.3 and a condensation temperature of 10 °C. According to the pseudo-adiabatic Rayleigh model (Noone, 2012; Smith, 1992), δD will decrease by about 120 ‰ if 70 % of the moisture rains out of the air parcel in its vertical accent during moist convection.

As a measure of the abundance of the D isotope relative to the ^{18}O isotope, deuterium excess of water vapor (dx), is formally defined as $dx = \delta D - 8 \times \delta^{18}O$. Here the factor 8 effectively removes the difference in equilibrium fractionation between D and ^{18}O, so dx is essentially controlled by kinetic fractionation (Merlivat and Jouzel, 1979). Equilibrium fractionation results from the lower saturation vapor pressures of HDO and $H_2{}^{18}O$ than that of H_2O, and kinetic fractionation from the fact that HDO and $H_2{}^{18}O$ have lower diffusion efficiencies in unsaturated air than H_2O. Unlike δD or $\delta^{18}O$ whose time variations are overwhelmed by Rayleigh distillation or rainout history of airmass advection, dx of atmospheric vapor is nearly constant during the transport of an airmass.

The dx observed in the atmospheric boundary layer (ABL) is sensitive to kinetic fractionation and can change if the water source region changes, that is, if the air is advected from a different region. Changes to dx at a fixed location can also occur if the air comes from the same source but the relative humidity (RH) and surface temperature at the

* Corresponding author.
E-mail address: zhongwang007@gmail.com (Z. Wei).

https://doi.org/10.1016/j.jhydrol.2019.123923
Received 7 March 2019; Received in revised form 23 May 2019; Accepted 3 July 2019
Available online 04 July 2019

Table 1
Summary of site information.

Site	Lon (°E)	Lat (°N)	Elevation (m)	Measurement Height	Sampling period	Data gap	dx (‰)		
				m			Min	Max	Ave
Mase	140.0	36.0	12	2–4	13-Jun-13 to 31-Aug-14	11-Nov-13 to 15-Jan-14	−1.7 (Jul)	31.9 (Jan)	17.9
Luancheng	114.7	37.8	50	1.6–4.3	1-Apr-08 to 14-Sep-08	–	−1.6 (Jul)	28.4 (May)	10.2
New Haven	−72.9	41.3	9	13	27-Mar-07 to 31-12-07	–	−5.7 (Jun)	43.6 (Nov)	21.0

source region changes (Simonin et al., 2014; Aemisegger et al., 2014). Since the dx is also slightly controlled by equilibrium fractionation (temperature dependence), the relative humidity is usually normalized by the saturation vapor pressure at the sea surface temperature. For example, a 20 % reduction in RH_{SST} at the ocean source increases the vapor dx by about 10 ‰; these changes are large, but predictable (Pfahl and Wernli, 2008; Uemura et al., 2012). A reproducible relationship between the dx and relative humidity near the ocean surface has been observed across a wide range of locations (Aemisegger et al., 2014; Pfahl and Sodemann, 2014; Pfahl and Wernli, 2008; Steen-Larsen et al., 2015; Uemura et al., 2008), although the impact of wind speed on the dx variation requires further clarification (Benetti et al., 2014; Lewis et al., 2013; Uemura et al., 2012). Given this relationship, dx is considered a good tracer of sea surface evaporative conditions and has been widely used to document oceanic sources of moisture (Delattre et al., 2015; Jouzel et al., 2013; Lewis et al., 2013; Masson-Delmotte et al., 2005; Merlivat and Jouzel, 1979; Yamanaka and Shimizu, 2007).

However, several studies have questioned whether the dx observed on land can be used as a conserved tracer of oceanic moisture sources (Aemisegger et al., 2014; Lai and Ehleringer, 2011; Parkes et al., 2017; Simonin et al., 2014; Welp et al., 2012; Zhao et al., 2014). A diurnal cycle of the dx near the land surface has been reported for a range of land surface types, implying a role of land evapotranspiration in modifying dx at the sub-day time scale (Berkelhammer et al., 2013; Simonin et al., 2014; Welp et al., 2012). Using dx measurements from six mid-latitude sites, Welp et al. (2012) showed that the dx near the ground surface can be significantly altered by local environmental conditions, including ABL height and local RH. Aemisegger et al. (2014) found that the dx value is inversely related to the RH at the land vapor source. Currently, isotope-enabled global circulation models (GCMs) can simulate dx over ocean surfaces reasonably well (Uemura et al., 2008), but generally have difficulty reproducing the dx observed on land, even for coastal and marine sites (e.g., (Steen-Larsen et al., 2017; Wei et al., 2016). One possible reason for the poor model performance is that these models do not account for the role of land surface evapotranspiration in controlling dx.

Moreover, dx of the near-surface vapor may be influenced by raindrop evaporation and by ABL entrainment. The kinetic effect of raindrop evaporation, which causes the vapor dx to increase, is mostly limited to the free atmosphere. Entrainment itself does not alter the total number of vapor isotopic molecules in the air column, but can change the near surface dx if the free atmospheric dx is different from the ABL dx. Although the community traditionally assumes that dx is the same between these two air layers (Gat, 2000), several observational studies indicate that dx in the free atmosphere is greater than that in the ABL (Bailey et al., 2013; Galewsky and Samuels-Crow, 2014; He and Smith, 1999).

In summary, temporal variations in the ABL dx observed at a fixed location on land represent a composite signal of multiple influences by remote moisture sources as well as processes in the local domain. An outstanding challenge is how to best isolate the role of non-local vapor sources and other local effects using the observed dx time series. To elucidate the mechanisms underlying the observed dx patterns, here we developed a process-based Lagrangian model for simulating dx at the hourly time resolution. This model was then used 1) to quantify how much information on initial conditions of remote oceanic moisture sources can be inferred from the dx observed at land sites, 2) to investigate the extent to which land evapotranspiration modifies the ABL dx, and 3) to determine if a suitable dx parameterization exists that can be used for land surface evapotranspiration.

2. Methods

2.1. Study sites

The dx data were obtained from three mid-latitude sites, including Luancheng in northeast China, Mase in central Japan, and New Haven in northeast US (Table 1). Although vapor isotope data are available for more than 30 sites (Wei et al., 2019), these three sites were selected for their special climatic conditions (continental, marine, and coastal). Luanchang is located in a landscape dominated by dryland crops (mainly wheat and corn) and at a distance of 270 km from the Yellow Sea. The Mase site is located on Tsukuba, Japan, at a distance of 30 km from North Pacific Ocean. New Haven is an urban site situated at a distance of 2.6 km from the Atlantic Ocean. Detailed information on the local climates, instrumentation and calibration protocols can be found in Wen et al. (2012) and Xiao et al. (2012) for Luancheng, Wei et al. (2016) for Mase and Welp et al. (2012) for New Haven. The original data were reported at hourly intervals. Here we used daytime (8:00–18:00) mean dx, a time period when the atmospheric boundary layer was well mixed.

2.2. Lagrangian vapor deuterium excess model

The backbone of our Lagrangian dx model is the trajectory model HYSPLIT (http://ready.arl.noaa.gov/HYSPLIT.php, version 4.0; Adler et al., 2003; Draxler and Hess, 1997; Stein et al., 2015) and the backward trajectory diagnostic algorithm proposed by Sodemann et al. (2008). Unlike Sodemann et al. (2008) and Pfahl and Wernli (2009), we do not use the diagnosed source regions to initialize an isotope model or to estimate dx from theoretical equations, but instead determine dx of the moisture source from a simple linear function of relative humidity (RH) at the source, with minor temperature and wind speed effects being ignored. In our model, dx is conserved during airmass advection, except when new vapor is added to the airmass by surface evaporation. Removal of moisture by precipitation does not change the dx. The effect of raindrop evaporation is also ignored.

Each backward trajectory was calculated for up to 10 days. The default forcing data was the GDAS (Global Data Assimilation System) data with $1^\circ \times 1^\circ$ spatial resolution and 3-h time resolution. We also forced the model with NCEP Reanalysis 2 with $1.75^\circ \times 1.75^\circ$ spatial resolution and 6-h time resolution. The trajectory release height was 500 m above the ground. Altogether, about 6560 trajectories were calculated for 820 measurement days with a total measurement duration of about 20,000 hr. Specific humidity, temperature and relative humidity of the air parcel at each trajectory time step were used to calculate the dx, as explained below.

The change in the specific humidity q between the two successive time steps along the backward trajectory was computed as (Fig. 1; Crawford et al., 2017, 2013; Pfahl and Wernli, 2008; Sodemann et al., 2008; Wei et al., 2018a):

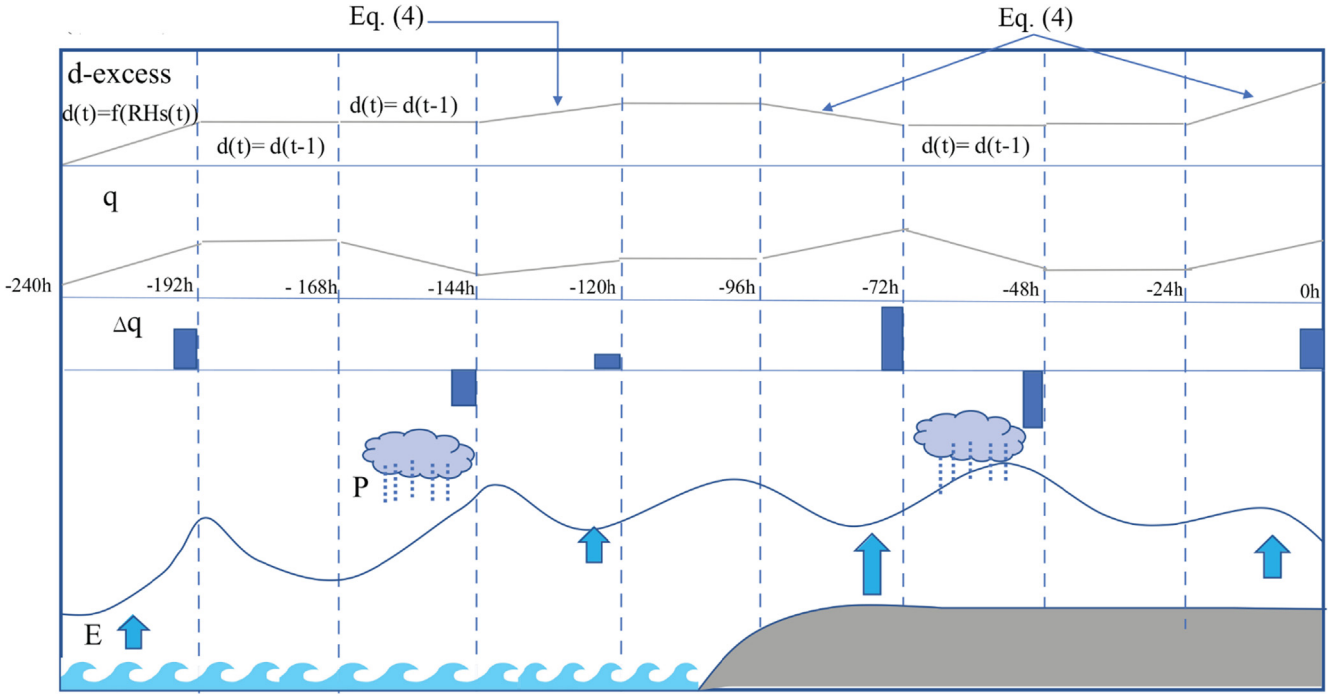

Fig. 1. A schematic diagram showing processes that influence the specific humidity and the vapor dx of an air parcel along a backward trajectory.

$$\Delta q(t) = q(\vec{x}(t)) - q(\vec{x}(t-\Delta t)) \quad (1)$$

where $\vec{x}(t)$ denotes the position of the air mass at time t, and Δt is either 3 h (GDAS) or 6 h (NCEP). If $\Delta q(t)$ (g kg^{-1}) is positive, moisture is taken up by the air parcel as a result of surface evaporation. If q is lower than 0.05 g kg^{-1}, the trajectory is terminated.

The dx of the air parcel is updated if Δq is positive to account for the influence of surface evaporation, using one of the seven parameterizations for the deuterium excess of evaporated vapor (Table 2). Parameterizations 1 to 3 consider only the influence of oceanic evaporation and omit the influence of land evapotranspiration, and parameterizations 4 to 6 include both effects.

In Parameterizations 1 to 3, ocean evaporation is the only source of moisture for the air parcel and precipitation is the only sink, and precipitation does not change dx along the trajectory (Fig. 1). The change in dx between two successive trajectory time steps is given by:

$$k(t) = x \bullet \frac{k(t-1) \bullet q(t)}{q(t-1)} + (x-1)[k(t-1) + \Delta q(t) \bullet dx_{SST}(t)] \quad (2)$$

$$dx(t) = k(t)/q(t) \quad (3)$$

where k (‰ g kg^{-1}) is an intermediate variable, x is a flag variable, and dx_{SST} (‰) is dx value of oceanic evaporation. Here x is equal to 1 for a grid marked as land surface, meaning that the dx of the air parcel remains unchanged, and is equal to 0 for a grid marked as ocean surface and $\Delta q(t) > 0$, meaning that oceanic evaporation contributes to a change in dx. Eq. (3) ensures isotopic mass balance by weighting specific humidity in each time step.

In Parameterizations 4 to 6, Eq. (2) is modified to:

$$k(t) = x \bullet \frac{k(t-\Delta t) \bullet q(t)}{q(t-\Delta t)} + (1-x) \times \begin{pmatrix} k(t-\Delta t) + \Delta q(t) \bullet dx_{sst}(t) \bullet (1 - LSF(t)) \\ + \Delta q(t) \bullet dx_{ls}(t) \bullet LSF(t) \end{pmatrix} \quad (4)$$

where x is equal to 1 for $\Delta q(t) \leq 0$ g kg^{-1} and 0 for $\Delta q(t) > 0$ g kg^{-1}. The grid flag LSF determines whether the change in q is caused by oceanic evaporation or land evapotranspiration. If LSF at time t is 0, Eq. (4) is reduced to Eq. (2). If $\Delta q(t) > 0$gkg^{-1} or the grid over which the parcel resides at time t is land, Eq. (4) becomes $k(t) = k(t-\Delta t) + \Delta q(t) \bullet dx_{ls}(t)$ where dx_{ls} (‰) is the dx value of land surface evapotranspiration.

Experimental studies show that the relative humidity RH_{SST} above the ocean surface in reference to the sea surface temperature (SST, °C) is highly anti-correlated with the dx of atmospheric water vapor over wide ranges of geographic and evaporation conditions (Angert et al., 2008; Pfahl and Wernli, 2008; Steen-Larsen et al., 2015, 2014; Uemura et al., 2008). A meta-analysis of these studies yields a mean relationship

Table 2
List of parameterizations and their assumptions. The mean bias index (BI), variations explained (R^2) and root mean square deviation (RMSD) are also shown for Mase (MS), Luancheng (LC) and New Haven (NH).

Parameterization	Forcing data	Ocean Evaporation	Land Evaporation	BI			R2			RMSD		
				MS	LC	NH	MS	LC	NH	MS	LC	NH
1	GDAS	dx = −54.0RHsst + 48.2	–	−4.47	−1.30	−2.15	0.65	0.19	0.17	7.42	5.18	8.20
2	GDAS	dx = −58.0RHsst + 51.0	–	−4.48	−0.62	−1.24	0.65	0.08	0.29	7.77	6.50	8.40
3	GDAS	dx = −42.6RHsst + 43.5	–	−7.36	2.97	−6.09	0.33	0.02	0.04	8.99	6.28	8.56
4	GDAS	dx = −54.0RHsst + 48.2	dx = −48.0RH + 54.9	−3.03	16.06	0.47	0.50	0.11	0.02	5.80	18.32	7.06
5	GDAS	dx = −54.0RHsst + 48.2	dx = −23.5RH + 35.2	−3.44	11.64	−0.27	0.50	0.11	0.05	5.79	12.67	5.88
6	GDAS	dx = −54.0RHsst + 48.2	Eq. (6) with NOAH E/ET	−3.68	5.07	13.78	0.49	0.06	0.11	6.52	7.38	19.54
7	NCEP	dx = -54.0RHsst + 48.2	–	−4.59	−3.23	−1.52	0.64	0.18	0.16	7.61	6.10	9.04

between dx of oceanic evaporation and RH_{SST},

$$dx_{SST} = -54.0RH_{SST} + 48.2, \quad (5)$$

(Pfahl and Sodemann, 2014). In this study, Eq. (5) is the default parameterization of the dx of the vapor evaporated from a marine source (Parameterization 1, Table 2).

The slope of the dx_{SST}versus RH_{SST} relationship may depend on season, measurement location and moisture transport path, showing a variation in the range of −43 to −58 ‰. For the purpose of sensitivity analysis, we have tested two more parameterizations for dx_{SST}, one with the most negative slope value ($dx_{SST} = -54.0RH_{SST} + 51.0$) provided by Uemura et al. (2008) (Parameterization 2) and the other with the least negative slope ($dx_{SST} = -42.6RH_{SST} + 43.5$) provided by Steen-Larsen et al. (2014) (Parameterization 3, Table 2).

In Parameterizations 4 and 5, the dx of land evapotranspiration is calculated with regression equations deduced from the site measurements, with local RH as the input variable (Section 3.4). Parameterizations 6 are based on the study by Aemisegger et al. (2014):

$$dx_{ls}(t) = -\frac{E(t)}{ET(t)}RH(t) + \frac{100E(t)}{ET(t)} \quad (6)$$

where dx_{ls} has the unit of ‰, E (Wm^{-2}) is soil evaporation and ET (Wm^{-2}) is total evapotranspiration (This equation is deduced from Aemisegger et al. (2014)'s Fig. 12). The ratio *E/ET* is obtained from the GLDAS Noah Land Surface Model V2 (NOAH LSM), for Parameterizations 6, with using RH from the GADS reanalysis. More detailed information can be found in Section 4.2.

2.3. IsoGSM simulation

We also compared the observed dx and the dx results from our trajectory model with those produced by the isotope-enabled global spectral model IsoGSM (Yoshimura et al., 2008). IsoGSM simulates the water vapor dx with a horizontal resolution of 1.75 degrees in six-hourly intervals. The data at the lowest grid height (2 m above the ground surface) are used for comparison. By using a spectral nudging technique, IsoGSM can reproduce reasonably well synoptic-scale variabilities of δD and $\delta^{18}O$ of the near-surface water vapor in coastal areas (Wei et al., 2016). A detailed description of the model configuration can be found in Yoshimura et al. (2008, 2014). The grid cells used here are centered at 138.75 E and 35.283 N, 114.375 E and 37.142 N, and −73.125 E and 40.952 N, corresponding to Mase, Luancheng and New Haven, respectively.

3. Results

3.1. Spatial and temporal variabilities of water vapor dx

Fig. 2 is an example showing evolutions of *q*, Δq and dx during a trajectory segment with the end time of 12:00 JST on September 20, 2013 and the end destination at Mase for Parameterizations 1 and 4. The specific humidity had a very low value at the start of the airmass transport (about 1.5 gkg^{-1} from −96 hr to −78 hr) from a land surface (Fig. 2a, black line). It became higher when the airmass passed over the ocean surface (−78 hr to −18 hr) and then was slightly depleted after the airmass had reached the land of Japan (−18 hr to 0 hr). The positive Δq was found mainly over the ocean grid points, suggesting that the moisture source was dominated by ocean evaporation (Fig. 2a, yellow line). Since there was no ocean source before −75 hr, Parameterizations 1 (black line in Fig. 2b) started at −75 hr. While for Parameterizations 4, it started at −96 hr. Compare to Parameterization 1, Parameterization 4 produced more variable dx because land surface evapotranspiration produced different dx from that of the ocean source.

Fig. 3 shows the variations in specific humidity (left panels) and dx (right panels) along back trajectories generated with Parameterization 1 for the three sites in August 2013 (Mase), August 2008 (Luancheng)

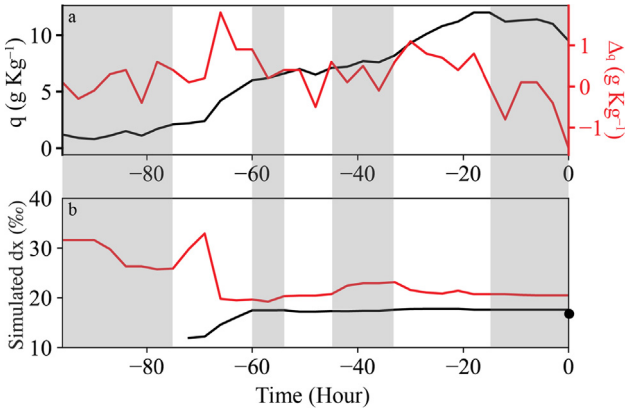

Fig. 2. Evolution of specific humidity q (black line in a), Δq (yellow line in a) and vapor dx using Parameterization 1 (black line in b) and 4 (red line in b) along the airmass back trajectory that ended at Mase site at 12:00, September 20, 2013. The grey areas represent travels over land surfaces. The black point represents the dx observed at the trajectory end time. (For interpretation of the references to colour in this figure legend, the reader is referred to the web version of this article.)

and August 2007 (New Haven). The monthly contribution from land or ocean was calculated by the sum of moisture coming from that region and was weighted by the specific humidity at destination for each trajectory. For all the sites, the specific humidity was initially low at the start of the airmass transport, and became higher if the airmass passed over the ocean area for most trajectories. For the Mase site, 88 % of the moisture came from the Pacific Ocean, with a secondary contribution (10 %) from land in North China and Mongolia (Fig. 3a). In contrast, for the Luancheng site (Fig. 3c), the dominant moisture came from interiors of North China (98 %), with only a minor contribution from the Pacific Ocean (2 %). For the New Haven site, the contribution of land sources was 67 % and that of ocean sources was 33 %. The simulation results show that changes in moisture source region were a driver of the dx variability. At Mase, water vapor originated from high-latitude ocean surfaces generally had a lower dx (6 to 14 ‰) than that from low-latitude ocean surfaces (12 to 22 ‰) (Fig. 3b). At New Haven, dx varied from 12 ‰ to 18 ‰ and 6 ‰ to 12 ‰ along the trajectories that originated from the North Atlantic Ocean and the Arctic Ocean, respectively (Fig. 3f). At Luancheng, the modeled dx was slightly higher than at New Haven, ranging from 8 ‰ to 20 ‰ (Fig. 3d).

Our trajectory results show that temporal variations in dx at Mase were closely related to changes in moisture source. The observed dx displayed a clear seasonal cycle, with the highest daytime mean in January (31.9 ‰) and the lowest daytime mean in July (−1.7 ‰; Table 1, Fig. 4). The back-trajectory analysis shows that the winter high dx was associated with high contributions to the local moisture from the Japan Sea, where low RH caused strong kinetic effects and high evaporation rates. In contrast, the warm-season low dx was associated with moisture originated from the low-latitude Pacific Ocean under conditions of high RH. This dichotomy of source region and dx between seasons suggests that the dx measured in marine climate may be a good tracer of moisture source. The dx measured in New Haven had a similar seasonal pattern as Mase, showing lower values in the warm season than in the cold season. The highest daytime mean value of 43.6 ‰ occurred in November, and the lowest value of 5.7 ‰ occurred in May. The moisture source in the winter season was dominated by high-latitude oceans with low RH thus leading to high dx, whereas the major moisture contribution for the summer season was the Atlantic Ocean. In comparison, the highest daytime mean value of the vapor dx at the Luancheng site occurred in May (28.4 ‰), and the lowest value occurred in July (−1.6 ‰), during the observation period (April to August). In-situ observations at Beijing at a distance of 270 km from Luancheng indicate high dx values in the winter months (Wen et al.,

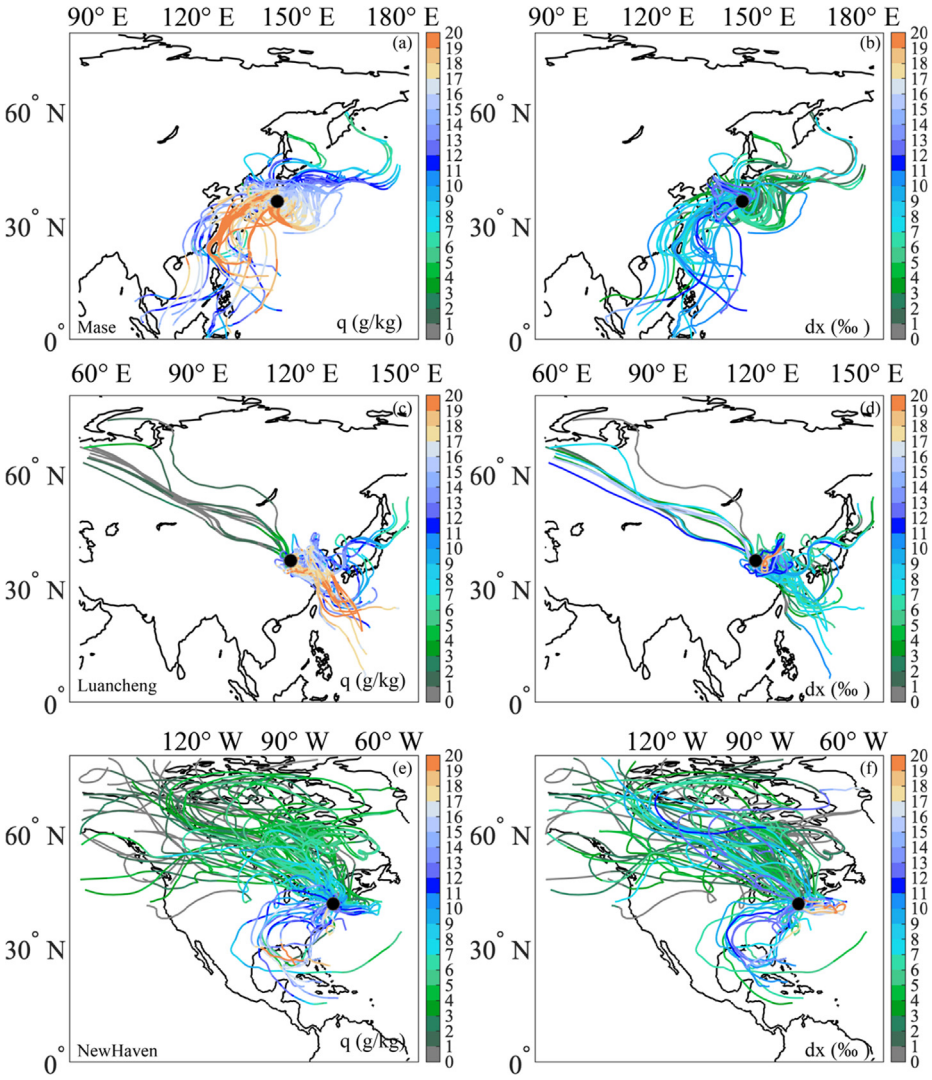

Fig. 3. Back trajectories generated for the three sites in August. The dx was calculated by the model with Parameterization 1. Color legends indicate specific humidity (left panels, g/kg) and dx (right panels, ‰). (For interpretation of the references to colour in this figure legend, the reader is referred to the web version of this article.)

2008), so it is possible that wintertime dx at Luancheng was also very high, but no direct observations existed in the winter to verify this seasonal pattern.

3.2. Comparison with observations

Parameterization 1 reproduced the observed water vapor dx well for the Mase site, with a high correlation of $R^2 = 0.65$ over the 12 months period. The performance was especially good for the warm seasons (the monsoon season; Fig. 4), which implies that our trajectory model captured reasonably well the influence of large-scale moisture advection on the water vapor dx variations. In contrast to the Mase site, the model was less successful for Luancheng. The model prediction shows a weak correlation with the observations at the New Haven site ($R^2 = 0.17$), although the simulated dx displays a clear seasonal cycle which is consistent with the observations. For all sites, the dx was underestimated, with a mean bias index (BI) of −4.47 ‰, −1.30 ‰ and −2.15 ‰ for Mase, Luancheng and New Haven, respectively (Table 2, Parameterization 1). It is noted that due to lack of contribution from oceanic sources, only a few daytime values (21 days) from the model with Parameterization 1 are available for comparison with observations at the Luancheng site.

The IsoGSM simulation failed to capture the dx variability at the inland site and was also systematically biased low for the marine and the coastal site. The R^2 values are 0.38, 0.17 and 0.01 for Mase, Luancheng and New Haven, respectively, and are lower than those for our trajectory model (Fig. 4). The BI (RMSD) values are −4.1 (6.5), 2.6 (3.3) and −4.1 (7.2) ‰ for Mase, Luancheng and New Haven, respectively. Bias errors are common in modeling studies on vapor isotopic compositions. So far, no atmospheric models are able to reproduce the water vapor dx temporal variabilities at hourly to daily time scales over the land surface.

3.3. Sensitivity to oceanic evaporation parameterization

As Table 2 and Fig. 5 shows, the R^2 value does not vary by much between Parameterization 1 and 2 for Mase ($R^2 = 0.65$), while Parameterization 3 gave less reliable results ($R^2 = 0.33$). Of the three parameterizations, Parameterization 3 was least sensitive to RH_{SST}; it gave slightly higher RMSDs (8.99 ‰ and 8.56 ‰ for Mase and New Haven, respectively) than the other two. Having the highest RH sensitivity, Parameterization 1 produced smaller RMSDs (7.42 ‰ and 8.20 ‰ for Mase and New Haven, respectively) than the other two. Parameterization 3 improved BI for Mase and Luancheng in the warm season (May to September) compared to Parameterization 1 but performed less well for the other season. For New Haven, Parameterization

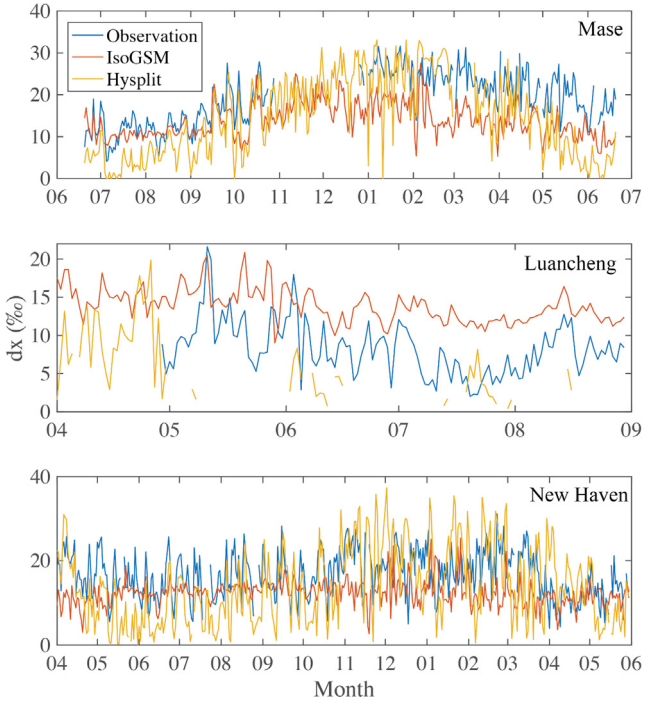

Fig. 4. Time series of daily dx observed, simulated by IsoGSM and calculated by the trajectory model with Parameterization 1.

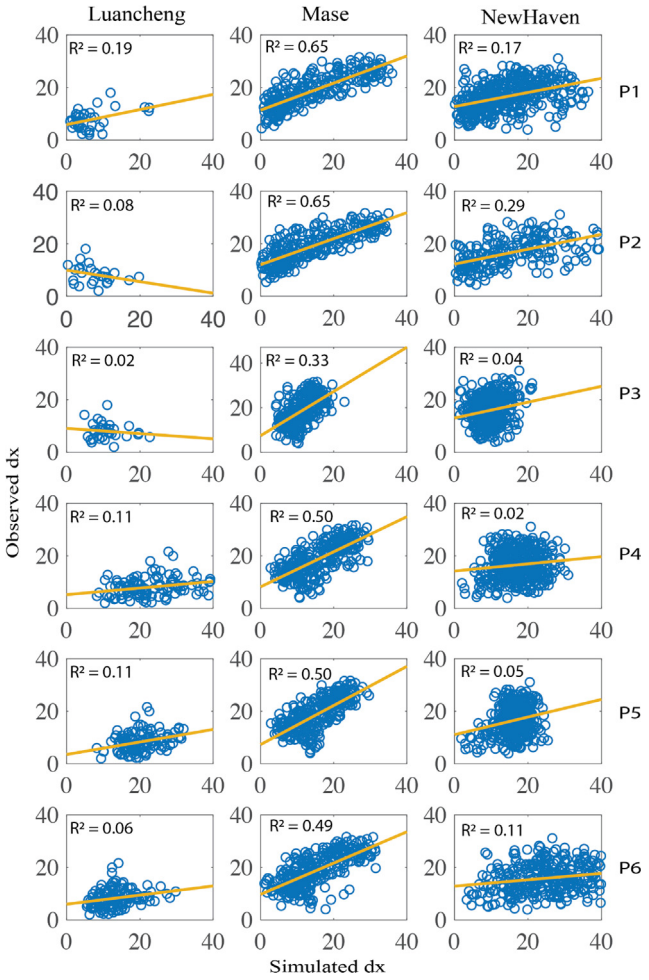

Fig. 5. Comparison of the observed dx with that simulated using the 6 evaporation dx parameterization schemes shown in Table 2.

3 had a positive BI. We conclude that the uncertainties associated with ocean evaporation dx estimation can bias the simulation results but likely play only a minor role in the overall model performance.

3.4. Sensitivity to land evapotranspiration parameterization

According to the experimental data, the daytime dx was correlated with local RH at New Haven (slope = −48.0 ‰ per %, $R^2 = 0.58$, $p < 0.001$) and Mase (slope = −23.5 ‰ per %, $R^2 = 0.22$, $p < 0.001$; Fig. 6a), suggesting that land ET contributions to the local atmospheric moisture were relatively high and that land surface ET should be considered in the dx simulation. The intercept and slope of the dx versus RH regression for New Haven and Mase seemed reasonable. When RH approaches 1, the regression predicts a dx of 11.7 ‰ and 8.9 ‰ for Mase and New Haven, respectively, which are close to the dx of local precipitation, implying that the vapor from ET was constrained the equilibrium fractionation. These slope values were lower than those reported for ocean evaporation, consistent with previous studies showing that water vapor originated from land has higher dx values than that from the oceans (Angert et al., 2008; Delattre et al., 2015; Gat and Matsui, 1991; Lai and Ehleringer, 2011; Welp et al., 2012).

As a sensitivity analysis, we parameterized the dx of land surface ET using these two regressions as represented by Parameterizations 4 and 5 in Table 2. These two parameterizations did not improve the overall R^2 and bias errors at Mase and New Haven, while they seemed to have improved the RMSD (Table 2). Previous studies have shown that dx may be enhanced by land surface evapotranspiration (Angert et al., 2008; Delattre et al., 2015; Gat and Matsui, 1991; Lai and Ehleringer, 2011; Welp et al., 2012). Consistent with this viewpoint, our land surface ET parameterization in Parameterizations 4 and 5 resulted in higher dx than that of ocean evaporation in Parameterizations 1, which may have contributed to the improved RMSD. As an example, Fig. 7 compared the R^2 and RMSD values between Parameterizations 1 and Parameterizations 4 at the monthly time scale. It is clear that for most of days, Parameterizations 4 improved the RMSD but worsened the R^2 (also see Table 2). A further investigation of the correlation pattern obtained with Parameterization 4 is given in Fig. 8. The strong negative relationship between R^2 and land surface fractional contribution to the atmospheric moisture indicates that land surface contribution should be the first-order factor affecting water vapor dx simulation in coastal and inland areas. It also suggests that the simple RH-dx relationship is not able to reproduce day-to-day variability of dx.

Parameterization 6, which considers the ET partitioning in land surface source dx estimation (Eq. (6)), it did not bring improvement over Parameterizations 4 and 5 (Table 2). Complete omission of land surface evapotranspiration as in Parameterizations 1–3, however, would make it almost impossible to predict dx at inland locations, such as the Luancheng site, where ocean sources are only minor contributors to the local atmospheric moisture. Nevertheless, the poor performance of Parameterizations 1–6 for Luancheng implies that additional processes must considered in the land surface evapotranspiration dx parameterization.

4. Discussion

4.1. Uncertainties in ocean evaporation dx estimation

In this study, the major environmental control of the dx of ocean evaporation is the SST-normalized relative humidity RH_{SST}. Some observational and modeling studies have shown evidence that wind speed can influence the RH_{SST} – dx relationship. The measurement over the subtropical Eastern North Atlantic Ocean showed that dx over the ocean surface depends on both relative humidity and surface wind speed (Benetti et al., 2014). By applying the closure assumption of Merlivat and Jouzel (1979), Aemisegger and Sjolte (2018) found very large

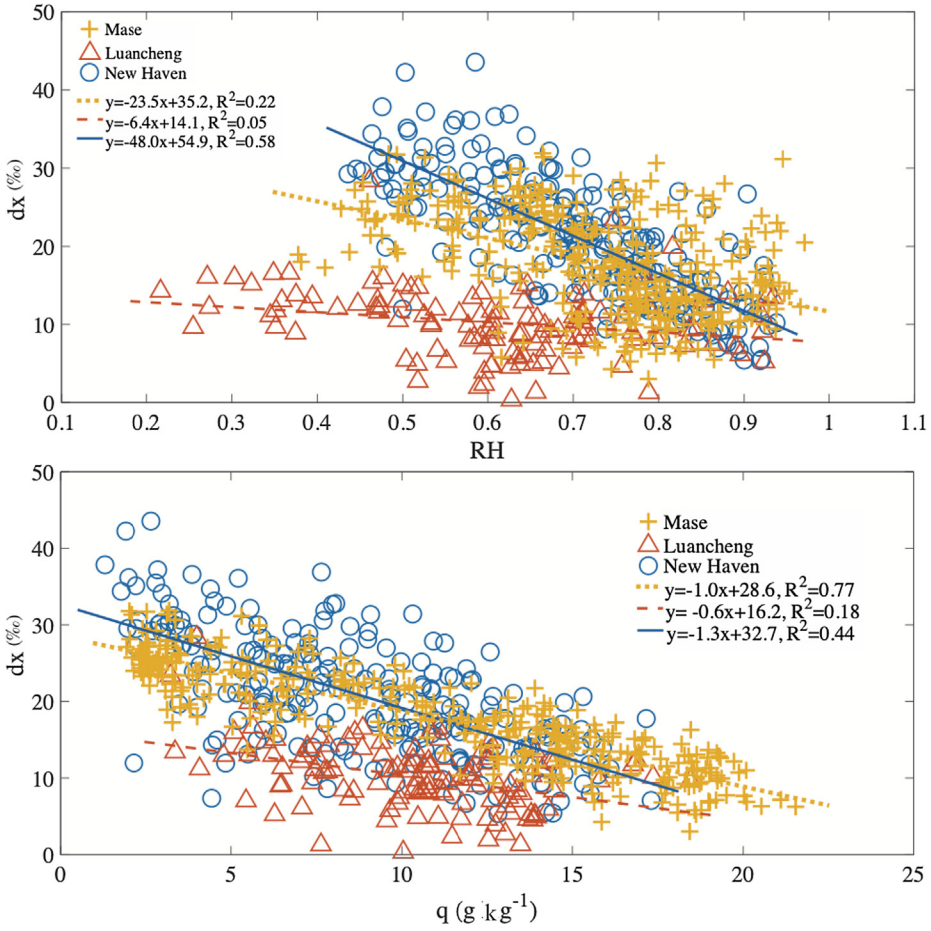

Fig. 6. Observed daily mean dx versus (a) local relative humidity RH and (b) local specific humidity q.

spatial variations in the RH_{SST} – dx slope due to spatial variations in wind speed. They showed that this slope becomes flat (slope value varies between −0.1 and −0.3 ‰ $\%^{-1}$) for high wind speed areas. Although our results (at least for the Mase site) are insensitive to the slope, it is possible that water vapor originating from extremely high wind ocean regions may have distinctive dx signatures. This conclusion is consistent with that from a new continuously measurement of both near-surface vapour and ocean surface water from the North Pole to Antarctica during a period of two years (Bonne et al., 2019), who suggested dx is controlled by RH_{SST} only.

In addition, sea ice may influence the RH_{SST} – dx slope. At the NEEM site in Greenland, high dx is associated with air masses that originate near the sea ice margin (Steen-Larsen et al., 2013). An isotope-enabled model simulation shows that the dx of water vapor is strongly affected by the sea ice extent in Antarctica area (Noone and Simmonds, 2004). When the humidity-depleted cold polar air masses cross the sea-ice margin (the open-water bodies), the strong evaporation results in large kinetic effects, leading to high observed d-excess of water vapor (Steen-Larsen et al., 2013). The sea ice impacts are negligible in the present study because few air mass trajectories passed the ice-cover oceans but should be addressed in future studies if the study site is at more northern latitudes and closer to ice-covered oceans.

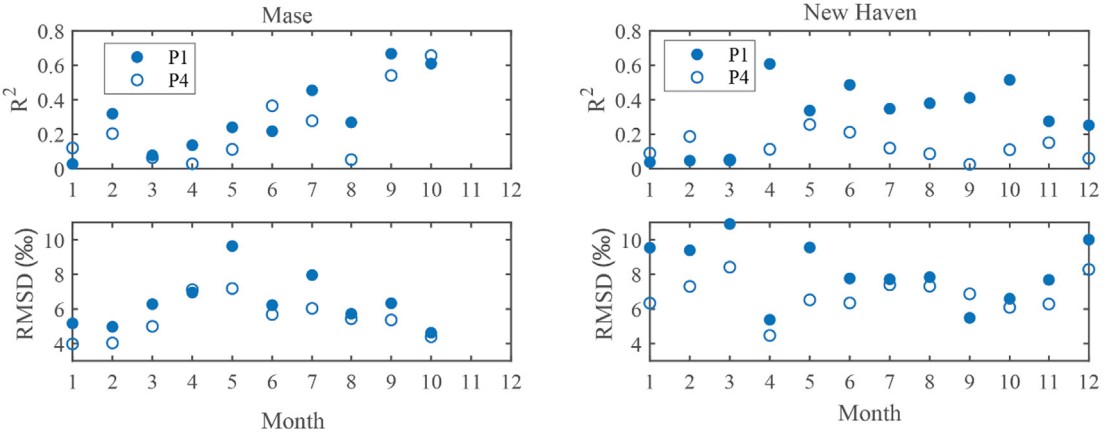

Fig. 7. The variation explained (R^2) by the trajectory model and the RMSD of the model result based on Parameterization 1 (P1) and Parameterization 4 (P4), for Mase (Left panel) and New Haven site (Left panel), respectively.

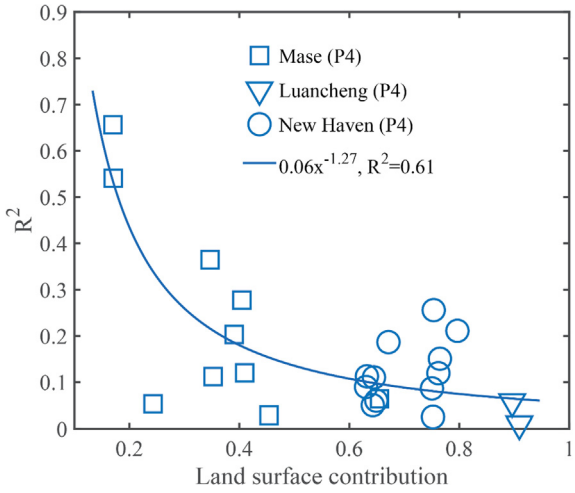

Fig. 8. Dependence between the variation explained by the model (R^2) on land surface contribution fraction, using Parameterization 4 (P4). Each data point represents data for one month.

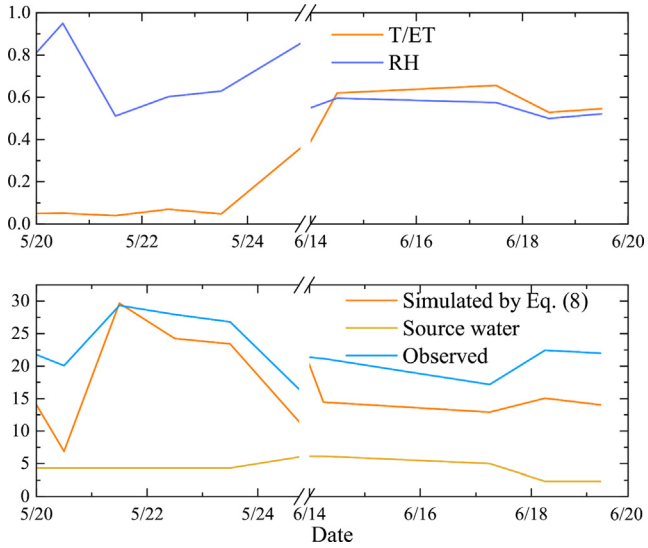

Fig. 9. Daily value of transpiration fraction T/ET and relative humidity RH (top), and d-excess of source water, water vapor from observation and from model simulation water vapor using parameterization Eq. (8) (bottom) for Mase site.

4.2. Uncertainties in the parameterization of dx of land evapotranspiration

Despite inclusion of the land ET effect on the vapor dx, Parameterizations 4 and 5 were not able to improve the simulations (Table 2 and Fig. 5). One potential reason is that the relationship between RH and the dx of land ET used by these parameterizations were valid in the local domain of the observational site but were not valid elsewhere along the airmass trajectory. A more general parameterization should express this relationship as a function of the trajectory timestep, as

$$dx(t) = aRH(t) + (dx_s(t) - a) \quad (7)$$

where a (< 0 ‰) is an empirical parameter which describes the maximum kinetic effect associated with evaporation, and dx_s is the dx of soil moisture. Parameterizations 1–3 imply that a is between −43 ‰ and −51 ‰. Eq. (7) satisfies two desired endmember properties. First, as RH approaches unity, the kinetic effect vanishes, and the dx of land ET approaches dx_s. Second, as RH goes to zero, Eq. (7) predicts that dx becomes to $dx_s - a$. In regions where the spatial variability of dx_s is negligible, the relationship between dx and RH established from local measurements can be used to calculate the dx of land evapotranspiration. Generally speaking, however, a single dx-RH relationship may not hold at all time steps of the trajectory calculation due to variable dx_s. In the case of Luancheng, the dx of soil moisture was highly variable in the source region where soil water in cropland in the summer growing season was a mixture of groundwater (via irrigation) and rainwater but soil water in the natural landscape comes only from rainwater. In this region, the groundwater has lower dx values (mean 5.1 ‰) than precipitation (mean 8.7 ‰; Wei et al., 2018b). The high spatial variability in dx may explain the poor correlation between the observed vapor dx and RH at Luancheng (Fig. 6).

An assumption implicit in Eq. (7) is that the land ET is dominated by soil evaporation. A further improvement to Eq. (7), inspired by Eq. (6), is to express the dx of land ET as a composite signal of transpiration and evaporation, as

$$dx(t) = \frac{dx_{root}(t)T(t) + [aRH(t) + dx_s(t) - a]E(t)}{ET(t)} \quad (8)$$

where dx_{root} (‰) is dx of soil moisture at the rooting depth. Since soil evaporation may play more important role than assumed by Aemisegger et al. (2014), it is essential to consider ET partitioning (ET = T + E) in the dx estimation. An isotopic large eddy simulation study showed that even a small evaporation contribution to ET can result in a large change of dx of the evapotranspiration isotopic composition (Wei et al., 2018c). A very high value of dx in the soil evaporation flux (75 ‰) was indeed used in computing the global E/ET based on catchment isotopic information (Jasechko et al., 2013). In Eq. (8), the dx value of transpiration is the same as that of soil moisture in the root zone.

Eq. (8) was tested for Mase, where high frequency isotopic measurements of both water vapor and surface water were available. We assumed that dx_{root} and dx_s are equal to the dx of the surface water, the slope parameter a was −54 ‰, and the evaporation ratio was calculated with a modified two-source Shuttleworth and Wallace ET model (Wei et al., 2018b). The time period was between Mary 20 and June 20, 2014. During this period, none of the parameterizations (Table 2) was able to reproduce the observed vapor dx variability (Fig. 4). The variabilities of T/ET and RH on the daily time scale are shown in Fig. 9. Water vapor dx generally depended on relative humidity, source water dx and T/ET. If By ignoring the contribution from ocean sources, parameterization Eq. (8) significantly improved the dx simulated with the trajectory model: the model now explains 71 % of observed variations in the vapor dx (R^2 = 0.71), which is much better that the R^2 of 0.22 using Parameterization 4 (Fig. 10).

The success of this new parameterization (Eq. (8)) at Mase has to do with the fact that the landscape upwind of the site was dominated by rice paddies and as such the dx_s value could be taken as a constant. More generally, the application of Eq. (8) requires detailed characterization of dx_s and E/ET fraction along the airmass trajectory. Such characterizations are not feasible from an observational point of view, but may be viable through a combination of isotope-enabled land surface modeling and atmospheric data assimilation.

4.3. Uncertainties from other sources

Parameterization 6 takes into account the different roles of transpiration and evaporation, while Parameterizations 4 and 5 do not. However, in addition to the drawbacks noted in the previous section, Parameterization 6 may be influenced by uncertainties in the E/ET estimation. In the present study, the E/ET data came from the NOAH land surface model imbedded in the Global Land Data Assimilation System Version 2. According to NOAH, on average, 50 % of land ET is attributed to soil evaporation, which is higher than the estimate (42 %) based on a recent study that combines data from multiple independent sources, including satellite-based estimations, reanalysis, land surface

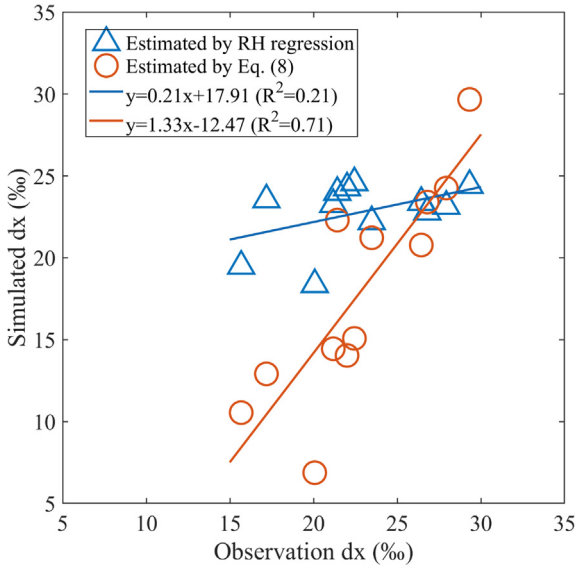

Fig. 10. Comparison of observed vapor dx and dx using two parameterizations (Eq. (8) and Parameterization 4) for Mase site from Mary 20 to June 20, 2014.

models, and isotopic measurements (Wei et al., 2017).

One source of uncertainties in our calculation is Lagrangian model itself. Our Lagrangian scheme assumes that the atmospheric residence time of moisture, or the mean residence time of moisture in the troposphere, of 10 days, (Trenberth, 1998; van der Ent and Tuinenburg, 2017; Yoshimura et al., 2004). Although an airmass may travel longer than 10 days over a continental region before arriving at the measurement site such as Luancheng, we were not able to extend the trajectory time period due to the substantial uncertainties in identifying source region for longer-range trajectories (Kahl, 1996; Rößler et al., 2017). In our study, the threshold value (0.05 g kg^{-1}) of specific humidity was applied in the trajectory length calculation. Wang et al. (2017) suggested a different threshold value (0.1 g kg^{-1}) for trajectory modeling. Their threshold value was also tested for the Mase site using Parameterization 1. The results show that the simulated dx is not sensitive to the selection of the threshold value of specific humidity, which is consistent with Wang et al. (2017). The model performance is almost the same using these two thresholds (R^2 = 0.64 (0.65) and RMSD = 7.64 (7.42) with 0.1 (0.05) g kg^{-1} specific humidity threshold). Sodemann et al. (2008) assumed that the trajectory was terminated if the air parcel has moved out of the planetary boundary layer (above the height of 850 hPa or 1500 m). Implementation of the boundary layer threshold did not improve model performance, with a slightly lower R^2 (0.62) and almost same RMSD (7.45) compared to the original calculation without a boundary layer threshold. By investigating individual events, Aemisegger et al. (2014) suggested that air parcels above the boundary layer can actually obtain moisture directly from surface evaporation. In our case, the humidity and boundary layer thresholds had limited effect on the dx simulation.

A second source of uncertainty of the Lagrangian model is that some physical processes may not be fully captured by the trajectory calculation, such as vertical convection and turbulent diffusion. The moisture content of an air parcel along a trajectory in the model world is also additionally altered by nonphysical factors such as numerical diffusion. However, these effects do not affect the source diagnostic strong enough to prevent the detection of physically reasonable correlations between the simulated and the measured isotopic compositions of water vapor (Pfahl and Wernli, 2008). That our trajectory model was able to reproduce the observed variability in specific humidity (e.g., R^2 = 0.93 for Mase site, Wei et al., 2016) implies that calculation of non-isotopic processes is not a prominent source of uncertainty for the isotopic simulation. A similar situation exists in the simulation with an isotope-enabled global circulation model, where the simulation shows very good agreement with observations for the specific humidity but not for dx of water vapor (Steen-Larsen et al., 2017; Wei et al., 2016).

To assess the potential errors caused by relative humidity, we repeated the model calculation by replacing the RH from the GDAS dataset with the RH from NCEP reanalysis-2, (Parameterization 7, Table 2). Compared to Parameterization 1, a slight improvement of BI was obtained, while R^2 for Mase site and New Haven site remained unchanged (Table 2). The improvement to BI was likely a result of lower RH in the NCEP reanalysis (1.8° × 1.8° resolution, with 6-hour interval) than that in the GDAS reanalysis (1° × 1° resolution, with 3-hour interval). A lower RH produces a higher dx of ocean evaporation, thus increasing the simulated dx of evaporated water vapor.

A final note of caution is that our trajectory model omits raindrop re-evaporation. It is known that the dx of water vapor is not conserved in an air parcel undergoing raindrop re-evaporation because the kinetic fractionation does not follow the 1:8 ratio for D and ^{18}O. In the extreme case where raindrops fall into completely dry air, laboratory experiments suggest that the evaporated vapor should have a dx value of 50 to 130 ‰ higher than that of the raindrop in its initial state (Stewart, 1975). In the real atmosphere, the dx enhancement depends on the fraction of raindrop evaporation and the RH below the cloud layer (Lee et al., 2009). Here we hypothesize that the direct effect of raindrop evaporation on the vapor dx is restricted to the free atmosphere where RH is much lower than in the ABL. Its effect on the ABL dx is probably indirect, occurring through the process of entrainment. It remains poorly understood as to how entrainment mixes the vapor isotopes between the ABL and the free atmosphere, primarily because the dx of the free atmospheric vapor is not known. Empirical evidence strongly suggests that water vapor in the free atmosphere should have higher dx than water vapor in the land ABL (Bailey et al., 2013; Galewsky and Samuels-Crow, 2014; He and Smith, 1999), most likely due to a larger role of raindrop evaporation in the free atmosphere. On the other hand, an evaporative model with a closure assumption and profiles of vapor dx observed over the subtropical Eastern North Atlantic Ocean (Benetti et al., 2014) and over Corsica during the HyMeX SOP1 campaign (Sodemann et al., 2017) suggest that the vertical profile of water vapor dx is more homogeneous than previously observed.

5. Conclusions

The trajectory model with Parameterization 1 reproduced reasonably well the daily vapor dx observed at the marine site (Mase), especially during ocean source dominated months. The results support use of a simple linear relationship with relative humidity as a parameterization of the dx of water vapor evaporated from the ocean surface. In contrast, the model performed poorly at the continental site (Luancheng; R^2 < 0.2). The model prediction shows a weak correlation with the observations at the coastal site (New Haven site; R^2 = 0.17), although the modeled seasonal pattern was consistent with that of the observation. On the monthly time scale, the model performance became worse as the fraction of land contribution to the atmospheric water vapor increased. The IsoGSM simulation failed to capture the dx variability at the continental site and was also systematically biased low for the marine and the coastal site.

Incorporation of parameterizations for the dx of land evapotranspiration suggested by previous studies did not bring obvious improvement to the simulation of the water vapor dx for these sites. The lack of improvement for Luancheng is particularly noteworthy because over 90% the atmospheric moisture at this site came from interiors of North China. We suggest that future improvement to the model requires us to overcome a fundamental challenge in isotopy hydrology, that is, the lack of understanding of the different fractionation processes of ^{18}O and D associated with land evapotranspiration.

Declaration of Competing Interest

The authors declare no competing interests.

Acknowledgements

This work was supported by the U.S. National Science Foundation (Grant AGS-1520684). All the data used in this study are available on request from the corresponding author. The authors gratefully acknowledge the NOAA Air Resources Laboratory (ARL) for the provision of the HYSPLIT transport and dispersion model and/or READY website (http://www.arl.noaa.gov/ready.php) used in this publication. The water vapor deuterium excess data is available at http://vapor-isotope.yale.edu/. The code used in this paper is available at https://github.com/zhongwangwei/iso_hysplit. SST data is available at https://www.esrl.noaa.gov. GLDAS Noah Land Surface Model L4 3-Hourly 1.0 × 1.0 degree is available at https://disc.gsfc.nasa.gov/datasets/GLDAS_NOAH10SUBP_3H_V001/summary?keywords=GLDAS.

References

Adler, R.F., et al., 2003. The version-2 global precipitation climatology project (GPCP) Monthly precipitation analysis (1979–present). J. Hydrometeorol. 4 (6), 1147–1167. https://doi.org/10.1175/1525-7541(2003) 004<1147:TVGPCP>2.0.CO;2.

Aemisegger, F., et al., 2014. Deuterium excess as a proxy for continental moisture recycling and plant transpiration. Atmos. Chem. Phys. 14 (8), 4029–4054. https://doi.org/10.5194/acp-14-4029-2014.

Aemisegger, F., Sjolte, J., 2018. a climatology of strong large-scale ocean evaporation events. Part II: relevance for the deuterium excess signature of the evaporation flux. J. Clim. 31 (18) 10.1175/JCLI-D-17-0592.1 7313-7336.

Angert, A., Lee, J.-E., Yakir, D.A.N., 2008. Seasonal variations in the isotopic composition of near-surface water vapour in the eastern Mediterranean. Tellus B 60 (4), 674–684. https://doi.org/10.1111/j.1600-0889.2008.00357.x.

Bailey, A., Toohey, D., Noone, D., 2013. Characterizing moisture exchange between the Hawaiian convective boundary layer and free troposphere using stable isotopes in water. J. Geophys. Res.-Atmos. 118 (15), 8208–8221. https://doi.org/10.1002/jgrd.50639.

Benetti, M., et al., 2014. Deuterium excess in marine water vapor: dependency on relative humidity and surface wind speed during evaporation. J. Geophys. Res.-Atmos. 119 (2), 584–593. https://doi.org/10.1002/2013jd020535.

Berkelhammer, M., et al., 2013. The nocturnal water cycle in an open-canopy forest. J. Geophys. Res.-Atmos. 118 (17), 10225–10242. https://doi.org/10.1002/jgrd.50701.

Bonne, J.-L., et al., 2019. Resolving the controls of water vapour isotopes in the Atlantic sector. Nat. Commun. 10 (1), 1632. https://doi.org/10.1038/s41467-019-09242-6.

Crawford, J., Hughes, C.E., Parkes, S.D., 2013. Is the isotopic composition of event based precipitation driven by moisture source or synoptic scale weather in the Sydney Basin, Australia? J. Hydrol. 507, 213–226. https://doi.org/10.1016/j.jhydrol.2013.10.031.

Crawford, J., Hollins, S.E., Meredith, K.T., Hughes, C.E., 2017. Precipitation stable isotope variability and subcloud evaporation processes in a semi-arid region. Hydrol. Process. 31 (1), 20–34. https://doi.org/10.1002/hyp.10885.

Delattre, H., Vallet-Coulomb, C., Sonzogni, C., 2015. Deuterium excess in the atmospheric water vapour of a Mediterranean coastal wetland: regional vs. local signatures. Atmos. Chem. Phys. 15 (17), 10167–10181. https://doi.org/10.5194/acp-15-10167-2015.

Draxler, R.R., Hess, G.D., 1997. Description of the HYSPLIT4 modeling system.

Galewsky, J., et al., 2016. Stable isotopes in atmospheric water vapor and applications to the hydrologic cycle. Rev. Geophys. 54 (4), 809–865. https://doi.org/10.1002/2015rg000512.

Galewsky, J., Samuels-Crow, K., 2014. Summertime moisture transport to the southern South American Altiplano: constraints from in-situ measurements of water vapor isotopic composition. J. Clim. https://doi.org/10.1175/jcli-d-14-00511.1.

Gat, J.R., 1996. Oxygen and hydrogen isotopes in the hydrologic cycle. Annu. Rev. Earth Planet. Sci. 24, 225–262. https://doi.org/10.1146/annurev.earth.24.1.225.

Gat, J.R., 2000. Atmospheric water balance—the isotopic perspective. Hydrol. Process. 14 (8), 1357–1369. https://doi.org/10.1002/1099-1085(20000615)14:8<1357::AID-HYP986>3.0.CO;2-7.

Gat, J.R., Matsui, E., 1991. Atmospheric water balance in the Amazon basin: an isotopic evapotranspiration model. J. Geophys. Res.-Atmos. 96 (D7), 13179–13188. https://doi.org/10.1029/91JD00054.

Good, S.P., Noone, D., Kurita, N., Benetti, M., Bowen, G.J., 2015. D/H isotope ratios in the global hydrologic cycle. Geophys. Res. Lett. 42 (12), 5042–5050. https://doi.org/10.1002/2015gl064117.

He, H., Smith, R.B., 1999. Stable isotope composition of water vapor in the atmospheric boundary layer above the forests of New England. J Geophys Res-Atmos 104 (D9), 11657–11673. https://doi.org/10.1029/1999jd900080.

Jasechko, S., et al., 2013. Terrestrial water fluxes dominated by transpiration. Nature 496 (7445), 347–350. https://doi.org/10.1038/nature11983.

Jouzel, J., et al., 2013. Water isotopes as tools to document oceanic sources of precipitation. Water Resour. Res. 49 (11), 7469–7486. https://doi.org/10.1002/2013wr013508.

Kahl, J.D.W., 1996. On the prediction of trajectory model error. Atmos. Environ. 30 (17), 2945–2957. https://doi.org/10.1016/1352-2310(96)00017-9.

Lai, C.T., Ehleringer, J.R., 2011. Deuterium excess reveals diurnal sources of water vapor in forest air. Oecologia 165 (1), 213–223. https://doi.org/10.1007/s00442-010-1721-2.

Lee, J.E., Johnson, K., Fung, I., 2009. Precipitation over South America during the last glacial maximum: an analysis of the “amount effect" with a water isotope-enabled general circulation model. Geophys. Res. Lett. 36 (19). https://doi.org/10.1029/2009gl039265.

Lewis, S.C., LeGrande, A.N., Kelley, M., Schmidt, G.A., 2013. Modeling insights into deuterium excess as an indicator of water vapor source conditions. J. Geophys. Res.-Atmos. 118 (2), 243–262. https://doi.org/10.1029/2012jd017804.

Masson-Delmotte, V., et al., 2005. GRIP deuterium excess reveals rapid and orbital-scale changes in greenland moisture origin. Science 309 (5731), 118–121. https://doi.org/10.1126/science.1108575.

Merlivat, L., Jouzel, J., 1979. Global climatic interpretation of the deuterium-oxygen 18 relationship for precipitation. J. Geophys. Res.-Oceans. 84 (C8), 5029–5033. https://doi.org/10.1029/JC084iC08p05029.

Noone, D., 2012. Pairing measurements of the water vapor isotope ratio with humidity to deduce atmospheric moistening and dehydration in the tropical midtroposphere. J. Clim. 25 (13), 4476–4494. https://doi.org/10.1175/Jcli-D-11-00582.1.

Noone, D., Simmonds, I., 2004. Sea ice control of water isotope transport to Antarctica and implications for ice core interpretation. J. Geophys. Res.-Oceans 109 (D7). https://doi.org/10.1029/2003JD004228.

Parkes, S.D., et al., 2017. Response of water vapour D-excess to land–atmosphere interactions in a semi-arid environment. Hydrol. Earth Syst. Sci. 21 (1), 533–548. https://doi.org/10.5194/hess-21-533-2017.

Pfahl, S., Sodemann, H., 2014. What controls deuterium excess in global precipitation? Clim. Past 10 (2), 771–781. https://doi.org/10.5194/cp-10-771-2014.

Pfahl, S., Wernli, H., 2008. Air parcel trajectory analysis of stable isotopes in water vapor in the eastern Mediterranean. J. Geophys. Res.-Atmos. 113 (D20). https://doi.org/10.1029/2008jd009839.

Pfahl, S., Wernli, H., 2009. Lagrangian simulations of stable isotopes in water vapor: an evaluation of nonequilibrium fractionation in the Craig-Gordon model. J. Geophys. Res. 114 (D20). https://doi.org/10.1029/2009jd012054.

Rößler, T., Stein, O., Heng, Y., Hoffmann, L., 2017. Regional and seasonal truncation errors of trajectory calculations using ECMWF high-resolution operational analyses and forecasts. Geosci. Model Dev. Discuss. 2017, 1–27. https://doi.org/10.5194/gmd-2016-314.

Simonin, K.A., et al., 2014. Vegetation induced changes in the stable isotope composition of near surface humidity. Ecohydrology 7 (3), 936–949. https://doi.org/10.1002/eco.1420.

Smith, R.B., 1992. Deuterium in North Atlantic storm tops. J. Atmos. Sci. 49 (22), 2041–2057. https://doi.org/10.1175/1520-0469(1992)049<2041:dinast>2.0.co;2.

Sodemann, H., et al., 2017. The stable isotopic composition of water vapour above Corsica during the HyMeX SOP1 campaign: insight into vertical mixing processes from lower-tropospheric survey flights. Atmos. Chem. Phys. 17 (9), 6125–6151. https://doi.org/10.5194/acp-17-6125-2017.

Sodemann, H., Masson-Delmotte, V., Schwierz, C., Vinther, B.M., Wernli, H., 2008. Interannual variability of Greenland winter precipitation sources: 2. Effects of North Atlantic Oscillation variability on stable isotopes in precipitation. J. Geophys. Res.-Atmos. 113 (D12). https://doi.org/10.1029/2007jd009416.

Steen-Larsen, H.C., et al., 2013. Continuous monitoring of summer surface water vapor isotopic composition above the Greenland Ice Sheet. Atmos. Chem. Phys. 13 (9), 4815–4828. https://doi.org/10.5194/acp-13-4815-2013.

Steen-Larsen, H.C., et al., 2014. Climatic controls on water vapor deuterium excess in the marine boundary layer of the North Atlantic based on 500 days of in situ, continuous measurements. Atmos. Chem. Phys. 14 (15), 7741–7756. https://doi.org/10.5194/acp-14-7741-2014.

Steen-Larsen, H.C., et al., 2015. Moisture sources and synoptic to seasonal variability of North Atlantic water vapor isotopic composition. J. Geophys. Res.-Atmos. 120 (12), 5757–5774. https://doi.org/10.1002/2015jd023234.

Steen-Larsen, H.C., Risi, C., Werner, M., Yoshimura, K., Masson-Delmotte, V., 2017. Evaluating the skills of isotope-enabled general circulation models against in situ atmospheric water vapor isotope observations. J. Geophys. Res.-Atmos. 122 (1), 246–263. https://doi.org/10.1002/2016jd025443.

Stein, A.F., et al., 2015. NOAA’s HYSPLIT Atmospheric Transport and Dispersion Modeling System. B Am. Meteorol. Soc. 96 (12), 2059–2077. https://doi.org/10.1175/BAMS-D-14-00110.1.

Stewart, M.K., 1975. Stable isotope fractionation due to evaporation and isotopic exchange of falling waterdrops - applications to atmospheric processes and evaporation of lakes. J. Geophys. Res. 80 (9), 1133–1146. https://doi.org/10.1029/JC080i009p01133.

Trenberth, K.E., 1998. Atmospheric moisture residence times and cycling: implications for rainfall rates and climate change. Clim. Change 39 (4), 667–694. https://doi.org/10.1023/a:1005319109110.

Uemura, R., et al., 2012. Factors controlling isotopic composition of precipitation on Okinawa Island, Japan: implications for paleoclimate reconstruction in the East Asian Monsoon region. J. Hydrol. 475, 314–322. https://doi.org/10.1016/j.jhydrol.2012.10.014.

Uemura, R., Matsui, Y., Yoshimura, K., Motoyama, H., Yoshida, N., 2008. Evidence of deuterium excess in water vapor as an indicator of ocean surface conditions. J. Geophys. Res.-Atmos. 113 (D19). https://doi.org/10.1029/2008JD010209.

van der Ent, R.J., Tuinenburg, O.A., 2017. The residence time of water in the atmosphere

revisited. Hydrol. Earth Syst. Sci. 21 (2), 779–790. https://doi.org/10.5194/hess-21-779-2017.
Wang, S., Zhang, M., Crawford, J., Hughes, C.E., Du, M., Liu, X., 2017. The effect of moisture source and synoptic conditions on precipitation isotopes in arid central Asia. J. Geophys. Res.-Atmos. 122, 2667–2682. https://doi.org/10.1002/2015JD024626.
Wei, Z., et al., 2016. Understanding the variability of water isotopologues in near-surface atmospheric moisture over a humid subtropical rice paddy in Tsukuba, Japan. J. Hydrol. 533, 91–102. https://doi.org/10.1016/j.jhydrol.2015.11.044.
Wei, Z., et al., 2017. Revisiting the contribution of transpiration to global terrestrial evapotranspiration. Geophys. Res. Lett. 44 (6), 2792–2801. https://doi.org/10.1002/2016gl072235.
Wei, Z., et al., 2018a. Influences of large-scale convection and moisture source on monthly precipitation isotope ratios observed in Thailand, Southeast Asia. Earth Planet. Sci. Lett. 488, 181–192. https://doi.org/10.1016/j.epsl.2018.02.015.
Wei, Z., et al., 2019. A global database of water vapor isotopes measured with high temporal resolution infrared laser spectroscopy. Sci. Data 6, 180302. https://doi.org/10.1038/sdata.2018.302.
Wei, Z., Lee, X., Patton, E.G., 2018c. ISOLESC: a coupled isotope-LSM-LES-cloud modeling system to investigate the water budget in the atmospheric boundary layer. J. Adv. Model Earth Syt. 10 (10), 2589–2617. https://doi.org/10.1029/2018MS001381.
Wei, Z., Lee, X., Wen, X., Xiao, W., 2018b. Evapotranspiration partitioning for three agro-ecosystems with contrasting moisture conditions: a comparison of an isotope method and a two-source model calculation. Agric. For. Meteorol. 252, 296–310. https://doi.org/10.1016/j.agrformet.2018.01.019.
Welp, L.R., et al., 2012. A meta-analysis of water vapor deuterium-excess in the mid-latitude atmospheric surface layer. Global Biogeochem. Cycles 26 (3). https://doi.org/10.1029/2011gb004246.
Wen, X.-F., et al., 2008. Continuous measurement of water vapor D/H and 18O/16O isotope ratios in the atmosphere. J. Hydrol. 349 (3–4), 489–500. https://doi.org/10.1016/j.jhydrol.2007.11.021.
Wen, X.-F., et al., 2012. Intercomparison of four commercial analyzers for water vapor isotope measurement. J. Atmos. Ocean Technol. 29 (2), 235–247. https://doi.org/10.1175/JTECH-D-10-05037.1.
Wright, J.S., et al., 2017. Rainforest-initiated wet season onset over the southern Amazon. Proc. Natl. Acad. Sci. U.S.A. 114 (32), 8481–8486. https://doi.org/10.1073/pnas.1621516114.
Xiao, W., Lee, X., Wen, X., Sun, X., Zhang, S., 2012. Modeling biophysical controls on canopy foliage water 18O enrichment in wheat and corn. Glob. Change Biol. 18 (5), 1769–1780. https://doi.org/10.1111/j.1365-2486.2012.02648.x.
Yamanaka, T., Shimizu, R., 2007. Spatial distribution of deuterium in atmospheric water vapor: diagnosing sources and the mixing of atmospheric moisture. Geochim. Cosmochim. Acta 71 (13), 3162–3169. https://doi.org/10.1016/j.gca.2007.04.014.
Yoshimura, K., Oki, T., Ohte, N., Kanae, S., 2004. Colored moisture analysis estimates of variations in 1998 Asian monsoon water sources. J. Meteorol. Soc. Jpn 82 (5), 1315–1329. https://doi.org/10.2151/jmsj.2004.1315.
Yoshimura, K., Kanamitsu, M., Noone, D., Oki, T., 2008. Historical isotope simulation using Reanalysis atmospheric data. J. Geophys. Res.-Atmos. 113 (D19), D19108. https://doi.org/10.1029/2008jd010074.
Yoshimura, K., Miyoshi, T., Kanamitsu, M., 2014. Observation system simulation experiments using water vapor isotope information. J. Geophys. Res.-Atmos. 119 (13). https://doi.org/10.1002/2014jd021662. 2014JD021662.
Zhao, L., et al., 2014. The patterns and implications of diurnal variations in the d-excess of plant water, shallow soil water and air moisture. Hydrol. Earth Syst. Sci. 18 (10), 4129–4151. https://doi.org/10.5194/hess-18-4129-2014.